Int. J. Electrochem. Sci., 12 **(2017)** 9335 – 9347, doi: 10.20964/2017.10.17

International Journal of
ELECTROCHEMICAL
SCIENCE
www.electrochemsci.org

Electrochemical Properties of Cellulose-nano-fiber/Reduced graphene oxide/Carbon-nano-tube Aerogel

Zihao Xu[1], *Chun Wei*[1,2,*], *Yongyang Gong*[1,2,*], *Jiayou Hu*[1], *Linlin Du*[1]

[1] College of Materials Science and Engineering, Guilin University of Technology, Guilin 541004, P. R. China
[2] Key Laboratory of New Processing Technology for Nonferrous Metals and Materials, Ministry of Education
[*]E-mail: 1986024@glut.edu.cn (C. Wei), yygong@glut.edu.cn (Y. Gong)

Received: 12 May 2017 / *Accepted:* 19 July 2017 / *Published:* 12 September 2017

Using the environmentally cellulose-nano-fiber as the precursor, we prepared a CNF/RGO/MWNT aerogel electrode material via mechanical blending and freeze-drying methods. The effect of RGO/MWNT content on the performance of the aeroge electrode was studied. The structure of the material was characterized with XPS and XRD. The electrochemical performance was characterized with an electrochemical workstation. The morphology was characterized by SEM. The results show that the CNF/RGO/MWNT aerogel electrode possessed good charge and discharge properties, and the specific capacitance increased firstly and then decreased with the increase the content of RGO. The internal resistance of the electrode material decreased with the increase of MWNT content. At a CNF/RGO/MWNT ratio of 30/40/30 and current density of 1 $A \cdot g^{-1}$, the specific capacitance reached a maximum of 88.08 $F \cdot g^{-1}$. After 1000 charge–discharge cycles, the capacitance retention rate was 95.4%, reflecting great stability. SEM results show that CNF was effectively incorporated into RGO/MWNT. The CNF/RGO/MWNT aerogel has a highly-connected three-dimensional porous network structure.

Keywords: cellulose-nano-fiber, graphene oxide, carbon-nano-tube, aerogel

1. INTRODUCTION

With the increase of wearable and portable electronic devices in nowadays, light-weight, high-power, high-energy-density, and environmentally has become the main demand of energy storage device. [1]. Super capacitor or electrochemical capacitor, as a novel energy-storage device, possesses

merits of high capacitance, long cycle life, wide working temperature range, etc., and has been extensively studied in recent years [2].

Graphene is a two-dimensional material, with a honeycomb-like structure, formed by the sp2 hybrid between carbon atoms. It has excellent electrical, optical, mechanical and electrochemical properties, Therefore, graphene-based porous carbon materials have been widely used in super-capacitor electrode materials [3, 4]. Carbon-nano-tube (CNTs) is a hollow columnar nanomaterial with great electrical conductivity, large specific surface area, and porosity for electrolyte ion transport. CNTs functioning as super-capacitor electrode materials can significantly improve the power density and cyclic stability [5]. However, in the process of preparation of electrode materials, adhesives and conductive agents such as polytetrafluoroethylene and acetylene black are added. These agents not only pollute environment, and at the same time are adverse to both the structure and performance of active species. Secondly, graphene and carbon-nano-tube are subject to agglomeration and stacking, which greatly limits the diffusion of electrolyte ions. Thereby, reducing the amount of binder and conductive agent, preventing the agglomeration of graphene and carbon-nano-tube, and increasing the wettability of graphene and carbon-nano-tube in electrolyte solutions are crucial to improving the electrochemical performance of super-capacitor [6, 7].

Cellulose-nano-fiber (CNF) is extracted from sustainable natural fibers. It has a high length/diameter ratio, great flexibility, great mechanical strength, and other excellent properties. Thanks to these virtues, CNF-based aerosol has a high porosity, low density, large specific surface area, and high adsorption capacity for electrolyte [8, 9].

In this paper, sisal CNF as the precursor, combined with graphene oxide (GO) and multi-walled carbon-nano-tube (MWNT) to prepare a CNF/GO/MWNT dispersion through sonication or mechanical stirring. Then, the dispersion was converted into CNF/GO/MWNT aerogels through a freeze-drying method and then converted into CNF/RGO/MWNT aerogels through a thermal reduction method. The CNF/RGO/MWNT aerogels were used as flexible super-capacitor electrode materials. The effect of RGO/MWNT mass ratio on the electrochemical properties of CNF/RGO/MWNT aerogels was studied. This work presents a possible application of CNF to super-capacitor electrode materials.

2. EXPERIMENTAL SECTION

2.1 Experimental materials

Sisal fiber was purchased from Guangxi Sisal Group Company. Sisal Pulp (SP) was home-made from Sisal fiber. MWNT, 5–15 μm in length and 15–25 nm in diameter, purified by acid treatment. was purchased from Shenzhen Nanotechnology Company. GO: 1-1.2 nm in lamellar thickness, 0.2-10 μm in diameter, Shanghai Ashine Technology Development Co., Ltd. Sodium chloroacetate (ClCH2COONa, AR) was derived from Suzhou Huihai Composite Materials Co., Ltd. Hydrochloric acid (AR), sodium hydroxide (AR), sodium sulfide ($Na_2S \bullet 9H_2O$) (AR), anhydrous

acetic acid (AR), and anhydrous ethanol (AR) were obtained from Xilong Chemical Co., Ltd. Sodium chlorite ($NaClO_2$) (CP) was obtained from Tianjin Damao Chemical Reagent Corporation.

2.2 Preparation of CNF

As shown in Figure 1. About 6 g Sisal Pulp (SP) was soaked in 18 mL of 5 wt% NaOH (aq) at room temperature for 30 min. The treated SP was then placed in a 500-mL three-neck flask and 0.553 g of NaOH, 1.848 g of sodium chloroacetate, and 120.46 mL of anhydrous ethanol were added. The mixture was refluxed at 75 °C in a water bath for 3 h. After the reaction, the product was placed in filter cloth and rinsed with deionized water to remove free reagents until it became neutral. The neutral product was then mixed with 1000 mL of deionized water to form a suspension with concentration reaching 0.5–0.6%. After that, the suspension was placed in a high-speed mixer by stirring and shearing for 10 min, until a transparent gel-like dispersion was formed. Eventually, the dispersion was centrifuged at 12,000 rpm for 5 min in order to remove the macrofibril, the CNF suspension (0.2%) was obtained [10], and –COOH group were grafted on its surface. Furthermore, CNF suspensions were dried in a dryer at the temperature of 60 °C, producing 3.43 g dried CNF for a yield of 57.2%.

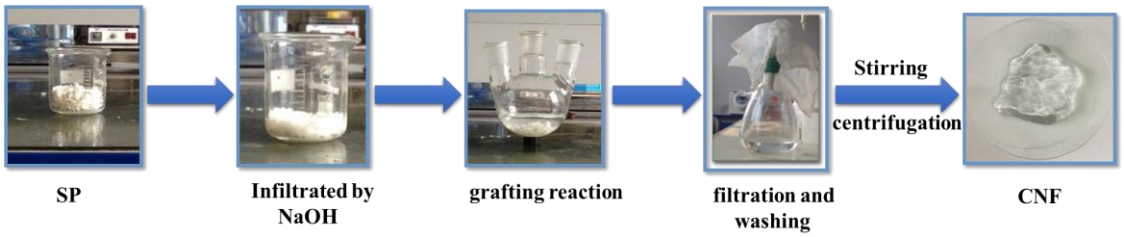

Figure 1. The production process of CNF

2.3 Preparation of CNF/RGO/MWNT aerogel

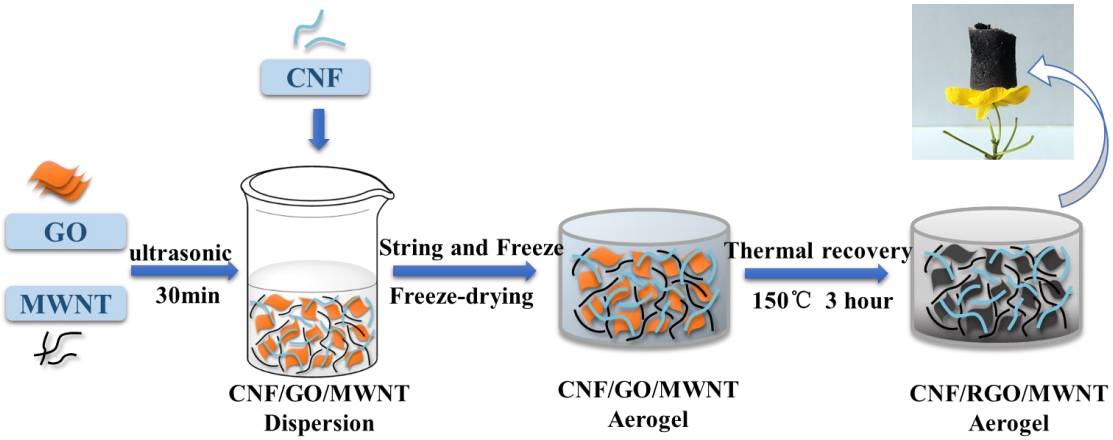

Figure 2. The Production Process of CNF/RGO/MWNT aerogel

As shown in Figure 2, at room temperature, different amounts of GO and MWNT (total mass was 1.167 g) were added to the 98.33 g of deionized water at mass ratios (GO to MWNT) of 0%/70%, 10%/60%, 20%/50%, 30%/40%, 40%/30%, 50%/20%, 60%/10%, 70%/0%, and the mixture was sonicated for 2 h. After the ultrasonication, 0.5 g of CNF was independently added to the GO/MWNT dispersions to form the CNF/GO/MWNT mixtures, and CNF was accounting for 30 wt% of the solute and 0.5 wt% of the solution. These CNF/GO/MWNT mixtures were then stirred in homogenizer (28000 rpm) for 30 min. The CNF/GO/MWNT dispersions were obtained. After that, the dispersions were froze for 12 h, and then were freeze-dried for 60 h to derive CNF/GO/MWNT aerogels. Finally, the CNF/GO/MWNT aerogels were heated at 150 °C in an oven for 3 h, GO was thermally reduced to RGO, then the CNF/RGO/MWN aerogels were obtained.

2.4 Preparation of CNF/RGO/MWNT aerogel electrode

In this experiment, rectangular stainless-steel-mesh pieces (4 cm × 1 cm) were employed as current collectors. The different amount of CNF/RGO/MWNT aerogels were separated into 1 cm × 1 cm × 0.2 cm cuboids (about 2 mg) and pressed onto the stainless-steel-mesh pieces at 2 MPa for 5 min, ensure that the stainless-steel-mesh pieces and aerogels have a tight connection. Then the loaded pieces were dried at 60 °C in oven for 6 h to prepare CNF/RGO/MWNT electrodes. Eventually, taking the quality of loaded pieces, make the quality of active material on a piece was 1–2 mg.

2.5 Characterizations of CNF/RGO/MWNT aerogels

The surface morphology of the samples was determined by scanning electron microscopy (SEM) with an AJSM-6380 LA scanning electron microscope. The samples were adhered to copper cylinder , coated with a thin layer of gold, and dried for the characterization. X-ray photoelectron spectroscopy (XPS) measurements for full spectrum and C1s spectra were conducted with an ESCALAB 250 (Thermo-VG Scientific Co., Ltd., the States, a A1-Ka target as the radiation source). X-ray diffraction (XRD) was performed with an X 'Pert PRO X-ray diffractometer (Netherlands, PANalytical B.V.) with a CuKα target as the radiation source, a tube voltage of 40 kV, a tube current of 40 mA, a scanning range of 5–70°, and a scanning rate of 5°/min.

2.6 Electrochemical performance characterization of CNF/RGO/MWNT aerogel

The electrochemical performance of the prepared electrode was tested with a ternary-electrode system in a CHI690 electrochemical workstation (Shanghai Chenhua Corporation). The working electrode was the CNF/RGO/MWNT aerogel electrode. The reference electrode was Ag/AgCl electrode. The counter electrode was Pt electrode. The electrolyte was a 1 mol/ L H_2SO_4 aqueous solution.

Cyclic voltammetry (CV) was conducted under the following conditions: a scan rate of 5, 10, 20, 50 and 100 mV/s in a voltage range of 0–1 V. Galvanostatic charge–discharge (GCD) experiments

were conducted at a constant current density (1000 mA/g), and the relationship of the potential against time was recorded to calculate the specific capacitance of electrodes following Eq. 2.1.

$$C = \frac{I\Delta t}{\Delta V} = \frac{I(t_2 - t_1)}{m(V_2 - V_1)} \quad \text{(Eq. 2.1)}$$

where c is the specific capacitance of discharge (F/g), I is the charge–discharge current during the test (A), m is the mass of active material in the electrode material (g), $\Delta t(t_2\text{-}t_1)$ is the discharge time (s), $\Delta V(V_2\text{-}V_1)$ is the voltage drop of discharge (V).

Electrochemical impedance spectroscopy (EIS) was performed as follows: an electrode was disturbed by AC voltage or current with small amplitude to derive the AC impedance data. Accordingly, an equivalent circuit would be simulated to calculate corresponding electrode reaction parameters. In the experiment, the frequency range was 0.01 Hz–100 KHz, the amplitude was 10 mV, the initial potential was 0 V, and the standing time was 2 s. Cycle stability of the CNF/RGO/MWNT aerogel electrode was tested by scanning 1000 times at a charge–discharge current density of 5000 mA/g, and calculated the relationship between the specific capacitance and number of cycles.

3. RESULTS AND DISCUSSION

3.1 XPS spectroscopy

Figure 3 shows the C1s XPS spectra of CNF/GO/MWNT and CNF/RGO/MWNT aerogels. The result of CNF/GO/CNT are shown in Figure 3a, four peaks corresponding to different carbon atoms are observed in the surface functional groups of the CNF/GO/MWNT aerogel. In detail, at 284.6 eV, the peak of un-oxidized carboatomic ring (C–C/C=C) is observed [11]. The peak at 286.0 eV corresponds to the hydroxyl and epoxy group (C–O) over CNF and GO [12]. Peaks of carbonyl (C=O) and carboxyl (O–C=O) are observed at ~288.9 and ~290.7 eV, respectively [13]. It is indicated that the CNF/GO/MWNT aerogel surface contains a large number of oxygen-containing functionalities, and the graphene oxide possessed a higher degree of oxidation.

The C1s spectrum of CNF/RGO/MWNT is depicted in Figure 3b. Except that the peak of un-oxidized carboatomic ring (C–C/C=C) is still intense at 286.4 eV, the other peaks in the spectrum of the CNF/RGO/MWNT aerogel are weakened or even disappear, compared to the spectrum of CNF/GO/MWNT aerogel [14]. It is implied that the carbon-ring structure of GO and MWNT was not destructed during the thermal reduction process, and the oxygen-containing functional groups on the GO were effectively removed [15]. The weak peaks corresponding to epoxy and hydroxyl groups are mainly attributed to the oxygen-containing functionalities in CNF.

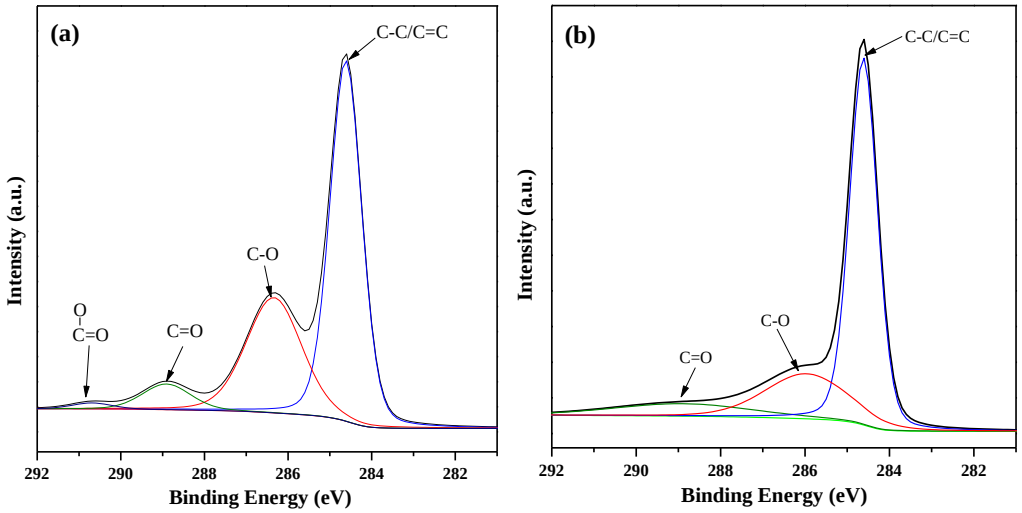

Figure 3. High-resolution XPS C1s spectra of (a) the CNF/GO/MWNT aerogel and (b) the CNF/RGO/MWNT aerogel

3.2 XRD spectroscopy

The XRD patterns of CNF, CNF/GO/CNT, and CNF/RGO/CNT are shown in Figure 4. In the pattern of CNF aerogel, an intense diffraction peak is observed at 2θ of 22.8°, corresponding to the (002) crystal plane of cellulose I [16]. The weak diffraction peaks at 2θ of 14.9°, 16.4°, and 34.4° correspond to the (101), (10$\bar{1}$), and (040) planes [17], respectively, indicating that the CNF prepared in the experiment has a cellulose-I-type crystal structure. In the XRD pattern of the CNF/GO/MWNT aerogel, the (002) plane diffraction peak of the cellulose-I is also observed at 2θ of 22.8°.

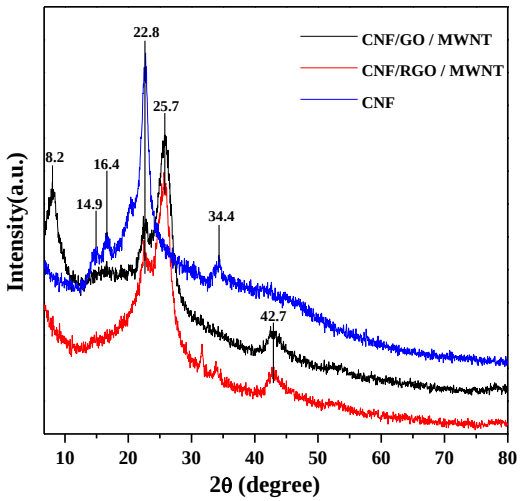

Figure 4. XRD patterns of the CNF, CNF/GO/MWNT and CNF/RGO/MWNT

Besides, another intense diffraction peak at 2θ of 8.2° corresponds to the (002) plane of GO [18]. The diffraction peaks at 2θ of 25.7° and 42.7° correspond to the (002) and (100) planes of MWNT, respectively [19]. The presence of CNF, GO, and MWNT is thus evidenced. The XRD

pattern of CNF/RGO/MWNT aerogel is similar to that of the CNF/GO/MWNT except that the (002) plane of GO at 8.2º is not observed in the former pattern, which indicates that GO was completely reduced to RGO during the thermal reduction process.

3.3 CV curve

The CV profiles of the CNF/RGO/MWNT aerogels are presented in Figure 5. In Figure 5a, which is the cyclic voltammetric curves of different proportion of CNF/RGO/MWNT aerogel electrodes in the same scanning rate of 10 mV/s, it can be seen that the area of the curve appears increasing first and then decreasing gradually with the increase of the RGO concentration. According to the equation: $C=S/(2\Delta V\nu)$ (C: specific capacitance, S: the enclosed area, ΔV: scanning window voltage, ν: voltage sweep rate), the specific capacitance is proportional to the enclosed area. Namely, the plot of specific capacitance of the CNF/RGO/CNT aerogel electrodes against the content of RGO also exhibits a behavior of increasing first and then decreasing. At CNF/RGO/MWNT mass fractions of 30%/40%/30% (hereinafter referred to as 30/40/30 CNF/RGO/MWNT), the specific capacitance reached a maximum.

The CV profiles of the 30/40/30 CNF/RGO/MWNT aerogel electrode at different scanning rates are illustrated in Figure 5b. It can be seen from the diagram, in the potential range of 0.0–1.0, there is no redox peaks are observed in CV curve, and the CV curve are rectangular and symmetric, with good symmetry, this showing thar the CNF/RGO/MWNT aerogel has ideal electric double layer capacitance. With the increase of scanning rate, the current increases accordingly, reflecting that the CNF/RGO/MWNT electrode can fast respond to a current. In addition, under the different scanning rates, these shape of the CV curve has not changed and deformed, indicating that the electrode can bear rapid and slow charge–discharge processes. The electrode has a good rate capability.

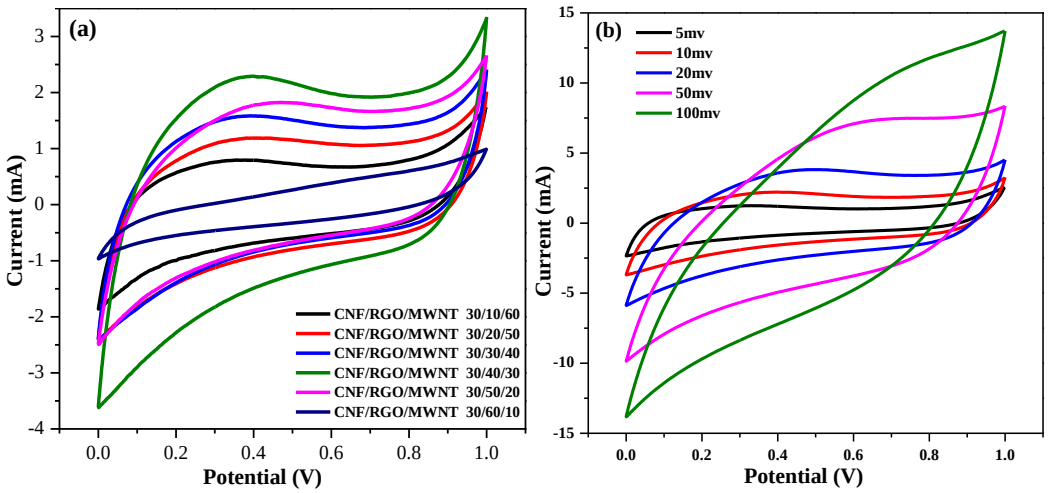

Figure 5. (a) The CV curves of various ratios of CNF/RGO/MWNT under the 10 mV/s voltage scan rate. (b) Typical cyclic voltammetry curves of 30/40/30 CNF/RGO/MWNT aerogel at different scan rates

3.4 GCD curve

The GCD curve of CNF/RGO/MWNT aerogel electrodes are illustrated in Figure 6. Figure 6a is the GCD curve of different content of CNF/RGO/MWNT aerogel electrodes under the current density of 1 A/g. In the range of 0.0-1.0 voltage, with the increase of RGO content, the charge–discharge duration exhibits the trend of increases at first and then decreases. According to equation 2.1, the specific capacitance is proportional to discharge time. Conversion for specific capacitance values as shown in figure 6b, it can be seen that the specific capacitance increased first and then decreased with increasing of RGO. When the CNF/RGO/MWNT mass fractions of 30%/40%/30%, the specific capacitance reaches a maximum of 88.09 F/g, which is consistent with the CV analysis results. Analyzing the reason, this is because when the RGO at a low concentration, the electrode material has a high porosity rate, and the number of ions transport paths in the electrolyte is increased. Hence, the specific capacitance increases with the increase of RGO. However, when the content of RGO is excessive, the excess of RGO will stack on the surface of the aerogel, blocking the three-dimensional porous network and thus decreasing the number of ion transport paths and the capacitance.

The GCD curves of 30/40/30 CNF/RGO/MWNT aerogel electrodes, at different current densities, are illustrated in Figure 6c. These curves are roughly symmetric and triangular, which indicating great reversibility, high charge–discharge efficiency, and good stability of the aerogel electrode. In the discharge process, a certain amount of pressure drop (IR drop) was observed, due to the Equivalent series resistance on the electrode [20]. The relationship of specific capacitance of the 30/40/30 CNF/RGO/MWNT aerogel electrode and the current density is shown in Figure 6d. As we can see, with the increase of current density, the specific capacitance was gradually reduced, for instance, when the current density is 0.5, 0.75 and 1.0 $A \cdot g^{-1}$, the specific capacitance is 143.60, 115.47 and 88.08 $F \cdot g^{-1}$ respectively. Compared to the specific capacitance of representative carbon-based electrodes, for example, Wang et al. [21] used the carbon nanotubes and reduction of graphene oxide to prepare the flexible electrode which was able to deliver 82.4 F/g. Cheng et al. [22] prepared the graphene and single-walled carbon nanotubes (SWCNT) composite film electrodes by a blending process, and the specific capacitance was 72.6 F/g in 1mol/L KCl solution.

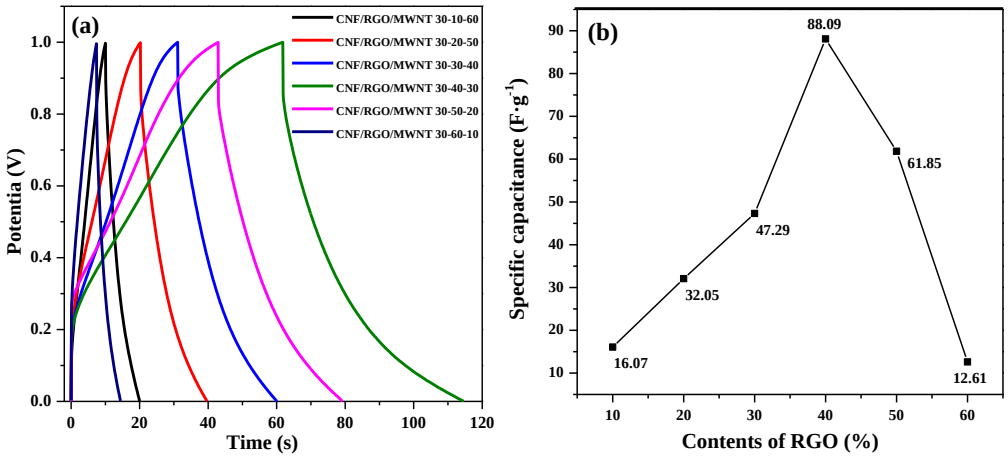

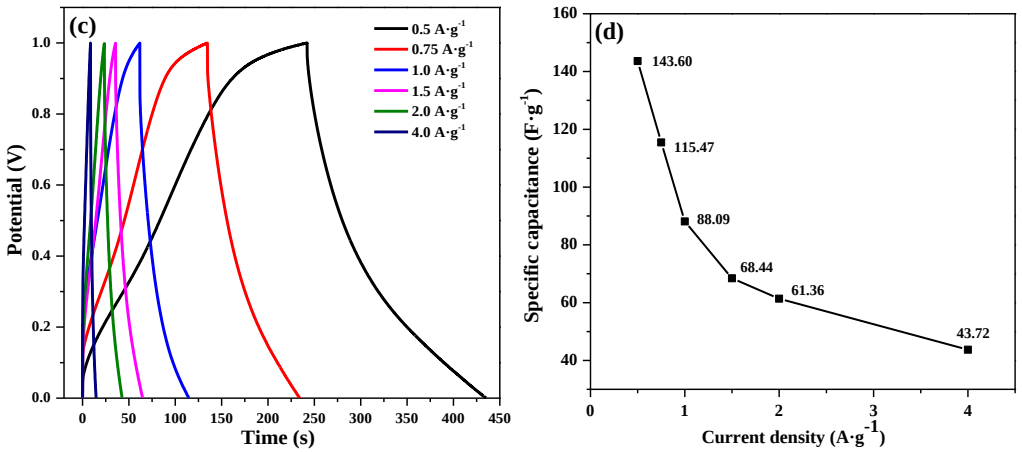

Figure 6. (a) The Charge-discharge curves of various ratios of CNF/RGO/MWNT at 1 $A \cdot g^{-1}$ current density (b) The specific capacitance of various ratios of CNF/RGO/MWNT (c) The Charge-discharge curves of 30/40/30 CNF/RGO/MWNT aerogel at different current densities (d) Dependence of specific capacitance on current density

Soo-Jin Park et al. [23] used carbon fiber and graphite nanofibers as electrode materials, the specific capacitance was 19 F/g and so force. Through the comparing, the CNF/RGO/MWNT aerogel electrode shows a relatively high capacitance value, which indicating that the three-dimensional porous network of the electrode can increase the number of ion transport paths and transport efficiency, effectively improve the specific capacitance of the material.

3.5 Cyclic stability

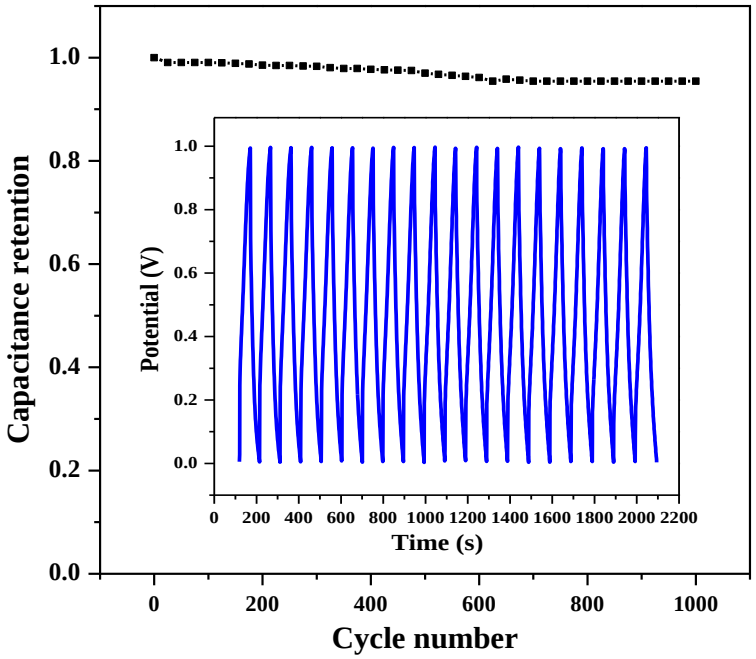

Figure 7. Cycling stability of 30/40/30 CNF/RGO/MWNT aerogel over 1000 cycles at a current density of 1 $A \cdot g^{-1}$

1000 charge–discharge cycles of the 30/40/30 aerogel electrode at current density of 1 $A \cdot g^{-1}$ are shown in Figure 7. The first 20 cycles are shown in the inset. It can be seen in 1000 times constant-current charge-discharge process, the capacitance retention rate of CNF/RGO/MWNT aerogel electrode slowed down, and finally to stabilize, the capacitance retention rate has descended from 100% to 95.4% in the end, which reflecting excellent stability. A possible reason is that the RGO and MWNT when used as super-capacitor electrode materials possessed the excellent cycling stability. Then, Another reason is due to the CNF/RGO/MWNT aerogel can form the three-dimensional porous network, which increases the transport rate and number of transport paths of ions and electrons in the electrolyte.

3.6 EIS curve

The Nyquist curves of CNF/RGO/MWNT aerogel electrodes with different compositions are illustrated in Figure 8. The figure shows that each curve consists of three parts, one part is a semicircle of the high-frequency region, the other part is a straight line in the medium-frequency region (a 45° angle between the line and x axis, due to the permeation–diffusion process of ions in the electrode), and another part is the straight line nearly parallel to the Y axis in the low frequency region. In the high-frequency region, the intercept of the curve intersecting with the real axis (Z') represents the resistance of the solution (R_S). Through the simulative equivalent circuit, which shows that the R_S value is 3.87 Ω. At the same time, the size of the semicircle represents the internal resistance of the ion transport in the system. In these Nyquist curves, with the increase of RGO content, the ion-transport internal resistance increases gradually, from 5.61 to 97.20 Ω, illustrates the electron transfer is slow. This is because along with the increase of the content of RGO, the content of MWNT is lower, and the MWNT content is the key factor improving the electrical conductivity, so the electrode material internal resistance increases, results in the decrease of electron transfer rate. In the low-frequency region, the curve is a similar to straight line, parallel to the Y axis, which reflects the behavior of an ideal electric capacity, which thanks to the three-dimensional porous network structure of the CNF/RGO/MWNT aerogel and the improved ion transport.

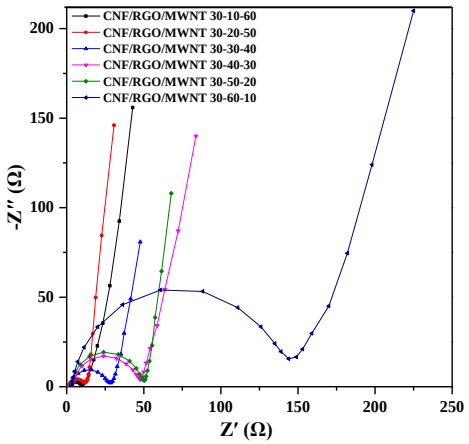

Figure 8. Nyquist impedance plots of the different contents of CNF/RGO/MWNT aerogel

3.7 SEM characterization

Figure 9 is the SEM of CNF/RGO/MWNT aerogel, The SEM image of un-pressed 30/40/30 CNF/RGO/MWNT aerogel is shown in Figure 9a. The figure shows that the aerogel is highly connected and has a three-dimensional porous network, with an average pore size of ~20 μm. These morphologies indicate that CNF, RGO, and MWNT formed a three-dimensional porous network in the freeze-drying process. The SEM image of 30/40/30 CNF/RGO/MWNT aerogel pressed at 2 MPa is shown in Figure 9b. It can be seen that the electrode surface remains the highly interconnected network of three-dimensional porous structure with pore size of 20~40 μm. It is because of this structure, increasing the transport paths of ions and enhances the wettability of electrode material in the electrolyte. However, the sizes and direction of pores are slightly deformed after subjected to high pressure, this due to the uneven pressure in the surface of electrode when in the process of film pressure.

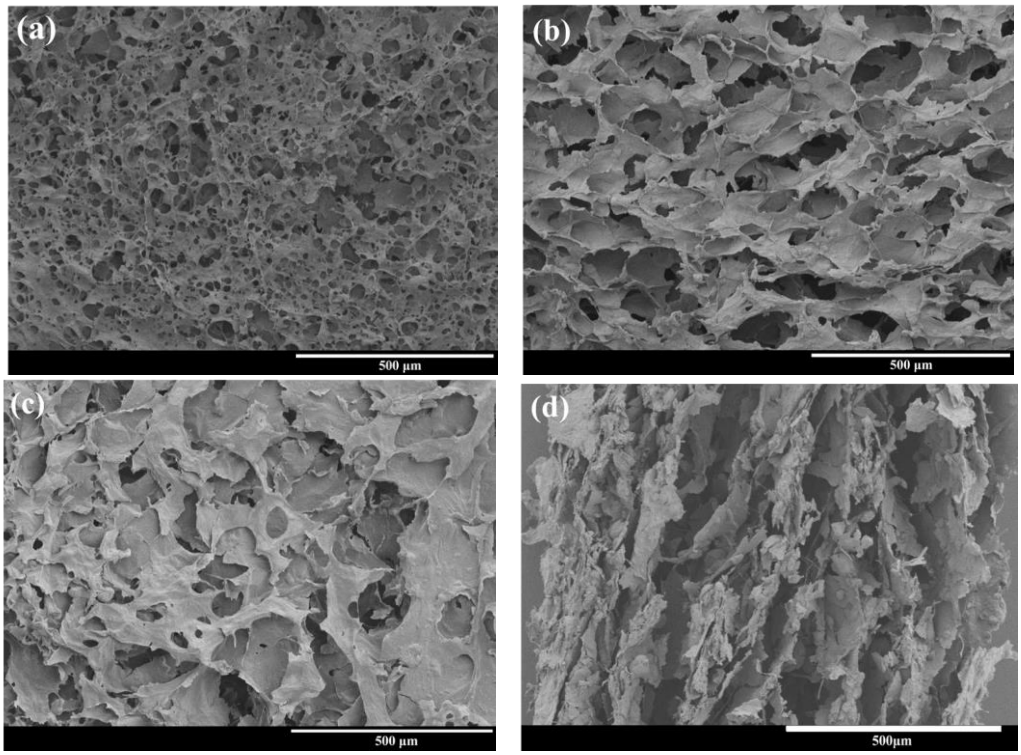

Figure 9. SEM images of the CNF/RGO/MWNT aerogel (a) 30/40/30 CNF/RGO/MWNT aerogel (b) 30/40/30 CNF/RGO/MWNT compressed aerogel (c) 30/50/20 CNF/RGO/MWNT compressed aerogel (d) cross-section of 30/40/30 CNF/RGO/MWNT aerogel

In comparison, the SEM image of 30/50/20 CNF/RGO/MWNT aerogel electrode (pressed at 2 MPa) is presented in Figure 9c. It can be seen that an excessively high content of RGO (see the left-bottom region of the image), the material still maintain three-dimensional porous network, but When RGO is more, RGO will stack on the surface. Thereby, the number of pores is reduced and the network is destructed. The ion transport paths will be blocked and thus the transport rate will be decreased. As such, the electrochemical performance will be worsened. The cross-sectional SEM image of 30/40/30 CNF/RGO/MWNT aerogel electrode (pressed at 2 MPa) is shown in Figure 9d. It can be seen that The

cross section has a lamellar and uniformly distributed structure, which is further reflecting the three-dimensional porous network structure of aerogel.

4. CONCLUSIONS

In this work, CNF/RGO/MWNT aerogels were successfully and separately prepared via freeze-drying and thermal reduction methods. The effect of RGO/MWNT content on the electrochemical properties of these aerogels was studied. The studies have shown that the CNF/RGO/MWNT aerogels have great reversibility and charge–discharge properties, and their specific capacitance exhibits increasing at first and then decreasing trend with the increase of RGO content. When the CNF/RGO/MWNT mass fractions of 30%/40%/30%, the specific capacitance reaches a maximum. At the current density of 0.5, 0.75, and 1 $A \cdot g^{-1}$, the specific capacitance values of the 30/40/30 CNF/RGO/MWNT aerogel are 143.60, 115.47, and 88.08 $F \cdot g^{-1}$, respectively. After 1000 times at a charge–discharge cycles, the capacitance retention rate is as high as 95.4%, exhibiting great stability.

ACKNOWLEDGEMENTS
The authors would like to acknowledge Guangxi Natural Science Foundation of China (Grant No.: 2016GXNSFAA380029).

References

1. J. A. Rogers, T. Someya and Y. Huang, *Science*, 327 (2010) 1603-1607.
2. P. Simon and Y. Gogotsi, *Nature materials*, 7 (2008) 845-854.
3. L. L. Zhang and X. Zhao, Chemical Society Reviews, 38 (2009) 2520-2531.
4. M. Pumera, *Energy & Environmental Science*, 4 (2011) 668-674.
5. Z. Fan, J. Yan, L. Zhi, Q. Zhang, T. Wei, J. Feng, M. Zhang, W. Qian and F. Wei, *Advanced materials*, 22 (2010) 3723-3728.
6. X. Yang, J. Zhu, L. Qiu and D. Li, *Advanced Materials*, 23 (2011) 2833-2838.
7. C. X. Guo and C. M. Li, *Energy & Environmental Science*, 4 (2011) 4504-4507.
8. H. Voisin, L. Bergström, P. Liu and A. Mathew, *Nanomaterials*, 7 (2017) 57.
9. Z. Yan, S. Chen, H. Wang, B. Wang, C. Wang and J. Jiang, *Carbohydrate Research*, 343 (2008) 73-80.
10. S. Wang, C. Wei, Y. Gong, J. Lv, C. Yu and J. Yu, *RSC Advances*, 6 (2016) 10168-10174.
11. S. Pei, J. Zhao, J. Du, W. Ren and H.-M. Cheng, *Carbon*, 48 (2010) 4466-4474.
12. W. Ye, X. Li, H. Zhu, X. Wang, S. Wang, H. Wang and R. Sun, *Chemical Engineering Journal*, 299 (2016) 45-55.
13. Y. Chen, X. Zhang, D. Zhang, P. Yu and Y. Ma, *Carbon*, 49 (2011) 573-580.
14. Z. Fan, K. Wang, T. Wei, J. Yan, L. Song and B. Shao, *Carbon*, 48 (2010) 1686-1689.
15. P. Cui, J. Lee, E. Hwang and H. Lee, *Chemical Communications*, 47 (2011) 12370-12372.
16. D. R. Biswal and R. P. Singh, *Carbohydrate Polymers*, 57 (2004) 379-387.
17. H. Zhao, J. H. Kwak, Z. Conrad Zhang, H. M. Brown, B. W. Arey and J. E. Holladay, *Carbohydrate Polymers*, 68 (2007) 235-241.
18. J. Shabani Shayeh, A. Ehsani, M. R. Ganjali, P. Norouzi and B. Jaleh, *Applied Surface Science*, 353 (2015) 594-599.
19. S. S. J. Aravind and S. Ramaprabhu, *RSC Advances*, 3 (2013) 4199-4206.

20. X.-L. Wu, T. Wen, H.-L. Guo, S. Yang, X. Wang and A.-W. Xu, *ACS nano*, 7 (2013) 3589-3597.
21. C. Yang, J. Shen, C. Wang, H. Fei, H. Bao and G. Wang, *Journal of Materials Chemistry A*, 2 (2014) 1458-1464.
22. Q. Cheng, J. Tang, J. Ma, H. Zhang, N. Shinya and L.-C. Qin, *Physical Chemistry Chemical Physics*, 13 (2011) 17615-17624.
23. L.-Y. Meng and S.-J. Park, *Materials Chemistry and Physics*, 132 (2012) 324-329.